Supporting Information

Constructing interspace in MnO@NC microspheres for superior lithium ion battery anode

Feiran Chen[†a], Zheng Liu[†a], Nan Yu[a], Hongxia Sun[a] and Baoyou Geng[*, a, b]

[a] College of Chemistry and Materials Science, The Key Laboratory of Electrochemical Clean Energy of Anhui Higher Education Institutes, Anhui Provincial Engineering Laboratory for New-Energy Vehicle Battery Energy-Storage Materials, Anhui Normal University, Wuhu, 241002, China.

[b] Institute of Energy, Hefei Comprehensive National Science Center, Anhui, Hefei, 230031, China.

Corresponding author: E-mail: bygeng@mail.ahnu.edu.cn

1. Experimental Section

1.1 Raw materials

All materials are purchased commercially without further purification. Hydrochloric acid (AR) and isopropanol (AR) are from Sinopharm Reagent Co., Ltd. Manganese sulfate (AR), dopamine hydrochloride (AR), gelatin (photographic grade), urea (AR), TEOS (AR), sodium hydroxide (AR) from Aladdin Reagent Co., Ltd. Tris (AR), sodium carboxymethyl cellulose CMC (AR), styrene butadiene rubber SBR (AR), ammonia (AR) are from Macleans Reagent Co., Ltd. Conductive carbon black (battery grade), lithium sheet (battery grade), copper foil (10mm), gasket (battery grade), spring sheet (battery grade), battery case 2032 (battery grade) and separator Celgard 2325 (battery grade) are from Nanjing Morges Co., Ltd.

1.2 Material preparation

Synthesis of MnO

0.338 g of manganese sulfate monohydrate was dissolved in 20 mL of water, and then 1.5 g of urea was dissolved in it and named solution A. Then 2.5 g of gelatin was dissolved in 20 mL of water, and the solution was named B. The solutions A and B were mixed uniformly at 40 °C, and then the mixed solution was transferred to the reactor and reacted at 140 °C for 12 h. After the reaction, the obtained product was washed three times with deionized water and absolute ethanol, and then the sample was dried overnight. Finally, the dried sample was calcined at 700 °C at 3 °C/min for two hours.

Synthesis of MnO@SiO_2

0.1 g of MnO was dissolved in a mixed solution of 80 mL of isopropanol and 20 mL of water, and stirred well. Then 2 mL of ammonia was added and stirred for 30 min, and finally 0.4 mL of TEOS solution was slowly added dropwise to the solution. After the solution was stirred for 12 h at room temperature, the product was washed three times with deionized water and absolute ethanol and dried to obtain MnO@SiO_2.

Synthesis of MnO@Void@NC

First, we separately prepared 0.1 mol/L tris and 0.1 mol/L HCl solutions, and then 50 mL of tris solution and 14.7 mL of HCl solution were mixed uniformly and transferred to a 100 mL volumetric flask for constant volume. After we obtained a hydrochloric acid buffer solution with PH=8.5. The MnO@SiO_2 obtained in the previous step was added to 40 mL of hydrochloric acid buffer solution and stirred evenly. Finally, 0.1 g of dopamine hydrochloride was added to the above solution and stirred for 12 h. The resulting black product was washed three times with deionized water and absolute ethanol. The dried product was calcined in a tube furnace at 600 °C for three hours at a heating rate of 2 °C/min. The calcined product was dissolved in 40 mL of 2 mol/L NaOH solution and stirred for 24 h, then washed with deionized water and absolute ethanol three times, and finally MnO@Void@NC was obtained.

Synthesis of MnO@NC

The prepared MnO was directly wrapped with dopamine and calcined, and finally the product MnO@NC was obtained.

1.3 Material characterization

We performed phase analysis (Bruker AXS, D8 Advance) of the material at 10-80° by X-ray powder diffractometer (XRD). The element valence state on the surface of the material was obtained by X-ray photoelectron spectroscopy (XPS) analysis (Thermo Fisher, ESCALAB 250XI). The morphology and structure of each sample were obtained by high resolution transmission electron microscope (HRTEM) (FEI, Talos F200x), transmission electron microscope (TEM) (Hitachi, HT-7700) and scanning electron microscope (SEM) (Hitachi, S-8100). The Raman spectra of the samples were obtained by laser confocal micro-Raman spectroscopy (SPEX, Ramanlog6). We used a thermogravimetric analyzer (TA, Q500) to test the thermogravimetry of the sample from 20-800℃ in air. The pores and specific surface area of the material were characterized by an automatic gas adsorption analyzer (McMurray ASAP2010N).

1.4 Electrochemical performance test

The battery was a 2032-type lithium ion battery assembled in a glove box in an Ar_2 environment. The test electrode material, conductive carbon black, CMC and SBR were mixed in a mass ratio of 7:2:0.5:0.5, and the evenly stirred slurry was coated on the copper foil. After the copper foil was

dried in a vacuum drying oven for 12 h, the circular electrode sheet was cut to assemble the battery. In addition, the load of the electrode sheet is 0.6-1.2 mg/cm^2. When assembled, we used EC: DEC with a volume ratio of 1:1 as the solvent, and dissolved 1M $LiPF_4$ as the electrolyte. At the same time, the microporous polypropylene film was used as the separator. The battery test was performed on the battery test system (Neware, CT-4008) with a range of 0.01 V to 3 V. On the workstation, the cyclic voltammetry curve was tested at a scan rate of 0.002 V/s in the range of 0.01-3 V, and the AC impedance test was also measured on the same workstation with an amplitude of 0.01 V from 0.1 MHz to 0.01 Hz.

2. Additional Figures

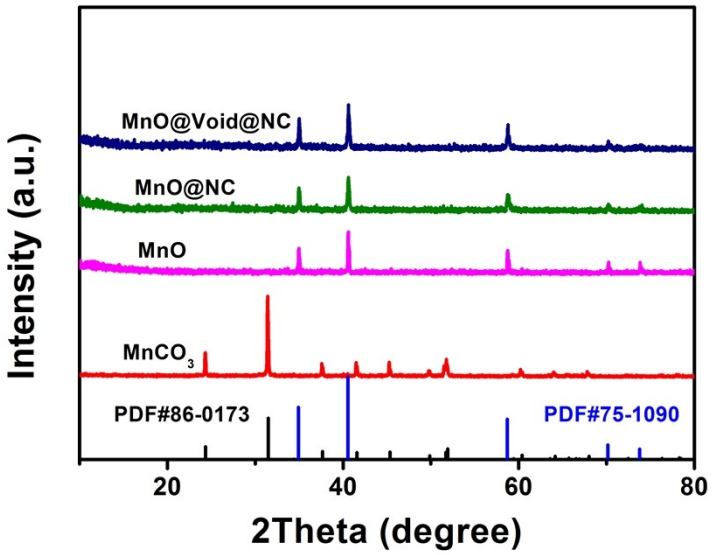

Figure S1. The XRD patterns of samples.

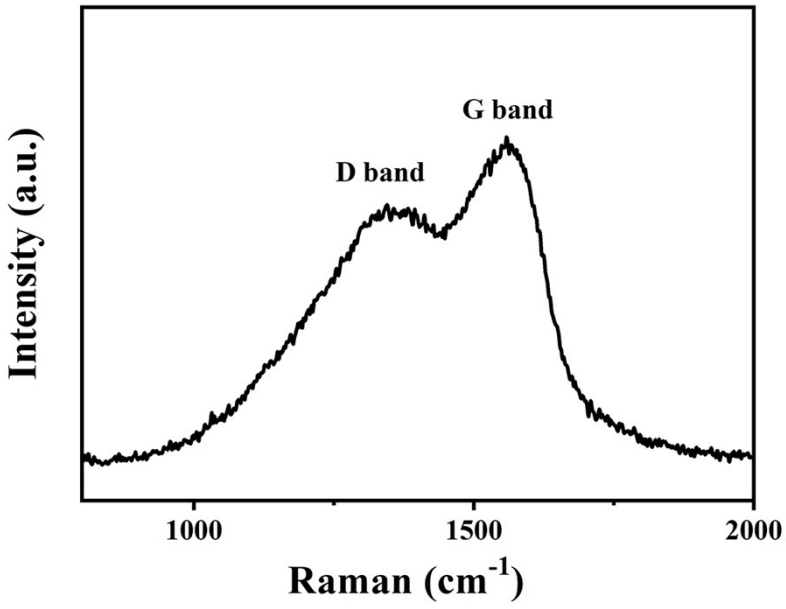

Figure S2. Raman spectrum of MnO@Void@NC.

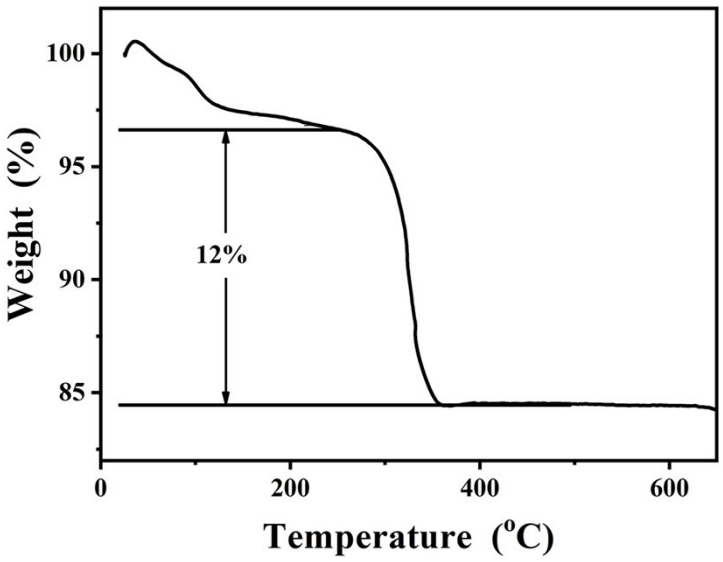

Figure S3. Thermo gravity analysis (TGA) curve of MnO@Void@NC under the air flow.

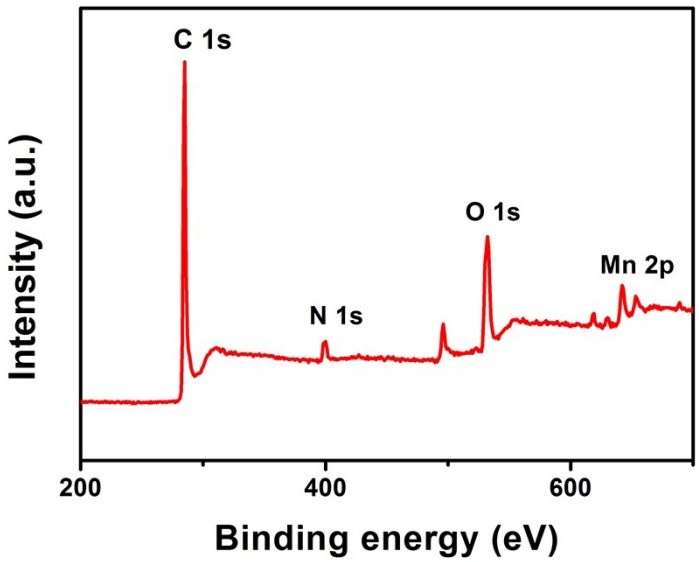

Figure S4. XPS spectrum of the sample MnO@Void@NC.

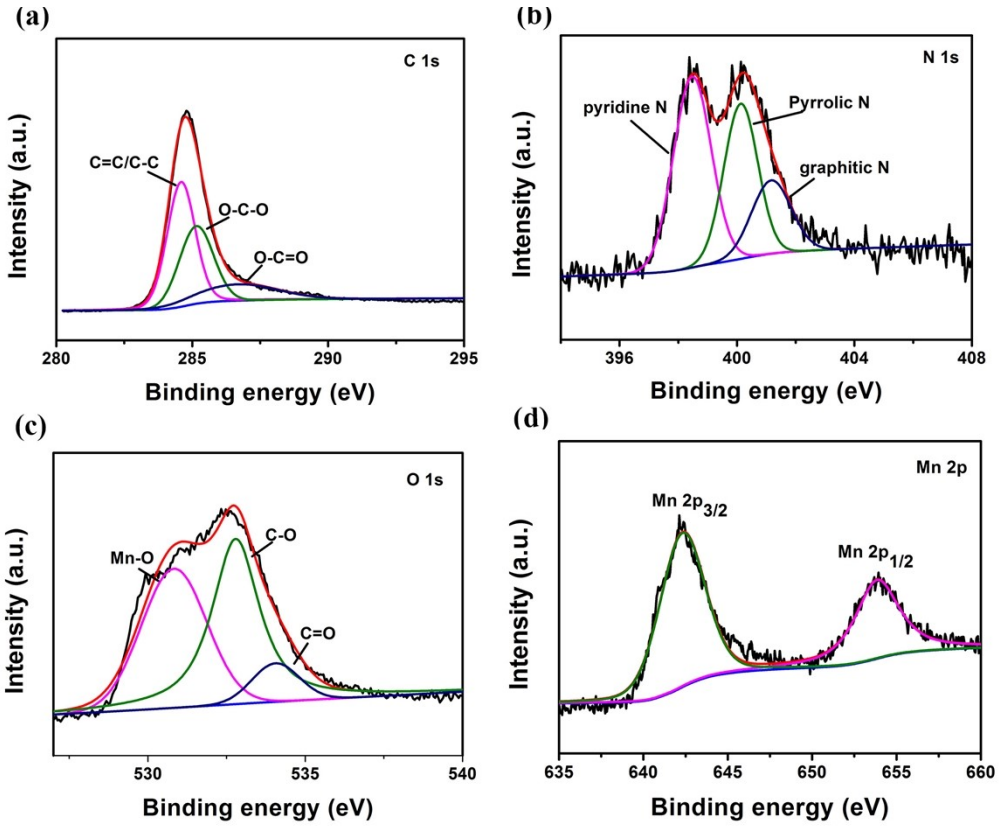

Figure S5. High-magnification XPS spectrums of MnO@Void@NC: (a) C 1s, (b) N 1s, (c) O 1s, (d) Mn 2p.

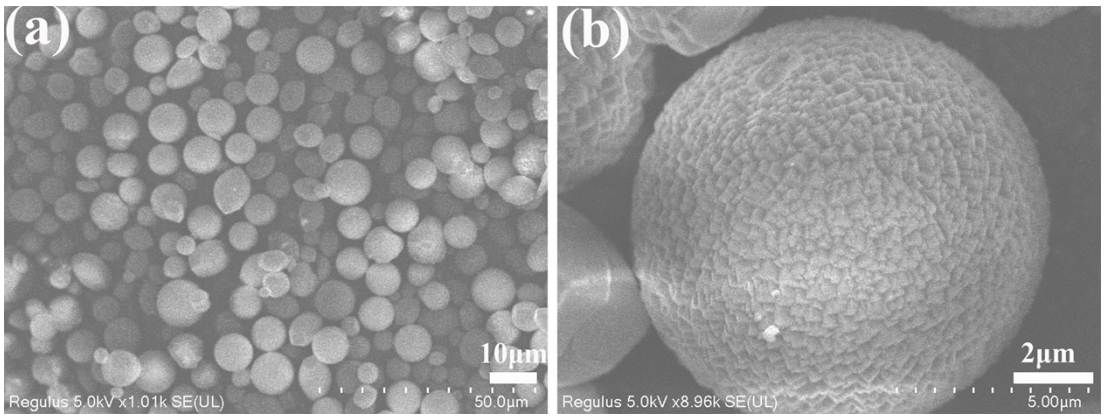

Figure S6. (a, b) SEM images of $MnCO_3$ under different magnifications.

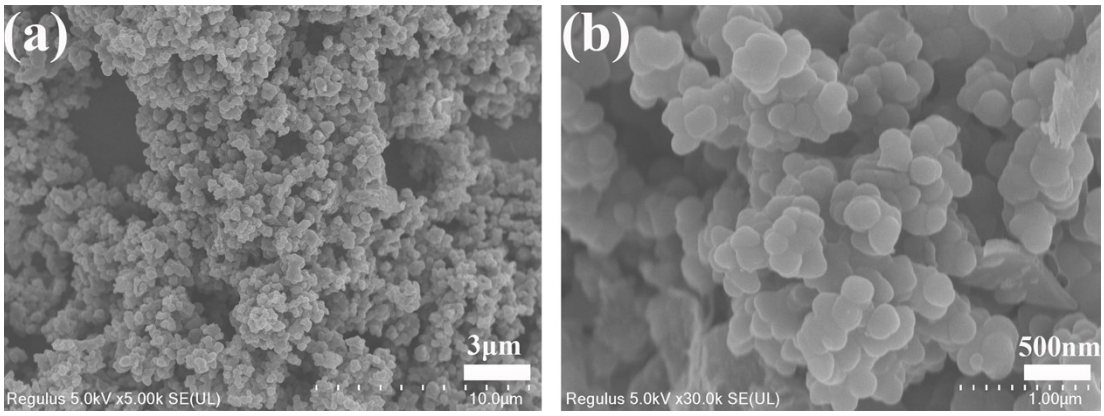

Figure S7. (a, b) SEM images of dopamine under different magnifications.

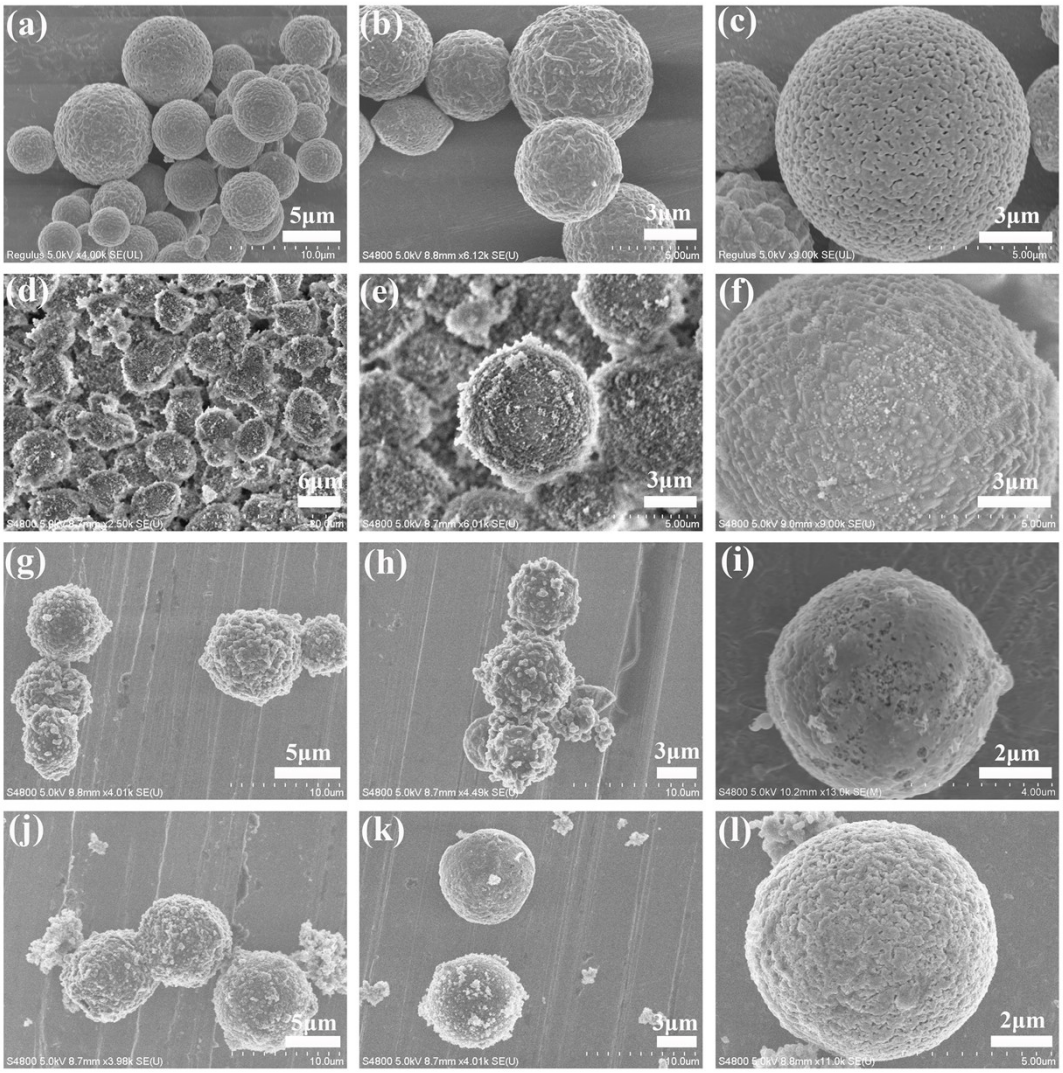

Figure S8. (a, b, c) SEM images of MnO under different magnifications, (d, e, f) SEM images of $MnO@SiO_2$ under different magnifications, (g, h, i) SEM images of MnO@NC under different magnifications, (j, k, l) SEM images of MnO@Void@NC under different magnifications.

Explanation: Figure S8 is the SEM image of each sample, Figure S8a-c shows the MnO microspheres calcined with $MnCO_3$ (Figure S6). It can be seen that the original morphology remains after calcination. The microspheres are generally around 5-9 μm. The surface of the microspheres is relatively rough after calcination. Figure S8d-f are SEM images of the sample $MnO@SiO_2$, it can be observed that many small-scale SiO_2 nanospheres grow on the surface of MnO microspheres. Figure S8g-i are SEM images of MnO@NC. It is formed by directly wrapping dopamine on the surface of MnO microspheres and then calcining. It can be observed that the microspheres are directly wrapped by a layer of carbon and nitrogen coating. The

inhomogeneous dopamine package and the incomplete carbonization of dopamine during calcination resulted in dopamine nanoparticles still on the surface of some of the microspheres shown in the figure. Figure S8j-l are SEM images of MnO@Void@NC. A small amount of dopamine nanoparticles also appears on the surface of MnO microspheres, which is the same as that of MnO@NC. However, the difference is that a large number of cavities are generated on the surface of the MnO microspheres, which are sufficient space positions when the MnO microspheres expand in volume during the charge and discharge process, thereby having excellent capacity and cycle stability.

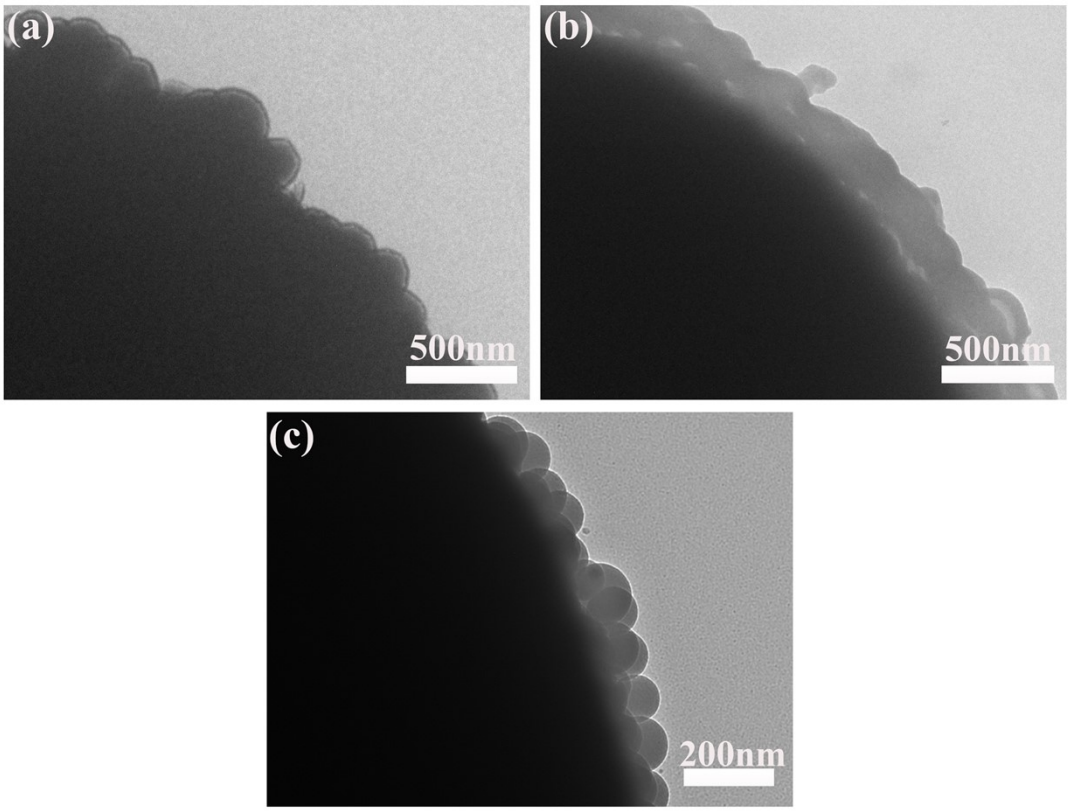

Figure S9. (a) TEM image of MnO, (b) TEM image of MnO@NC, (c) TEM image of $MnO@SiO_2$.

Explanation: Figure S9 is a TEM image of each sample. Figure S9a is the TEM image of the sample MnO. The microspheres are found to be solid through observation. Figure S9b is the TEM image of the sample MnO@NC. From the figure, it can be found that a layer of carbon-nitrogen structure appears at the edge, indicating that the surface of the MnO microspheres is evenly covered by the carbon layer. Figure S9c is the TEM image of the sample $MnO@SiO_2$. A large number of SiO_2 nanoparticles grow on the surface of MnO.

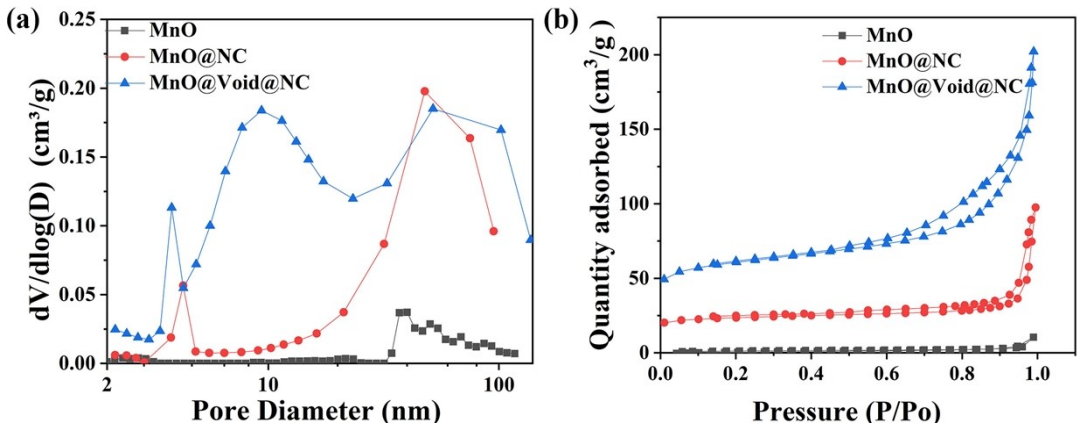

Figure S10. (a) Pore size distribution curve of samples; (b) N_2 adsorption–desorption isotherm of samples.

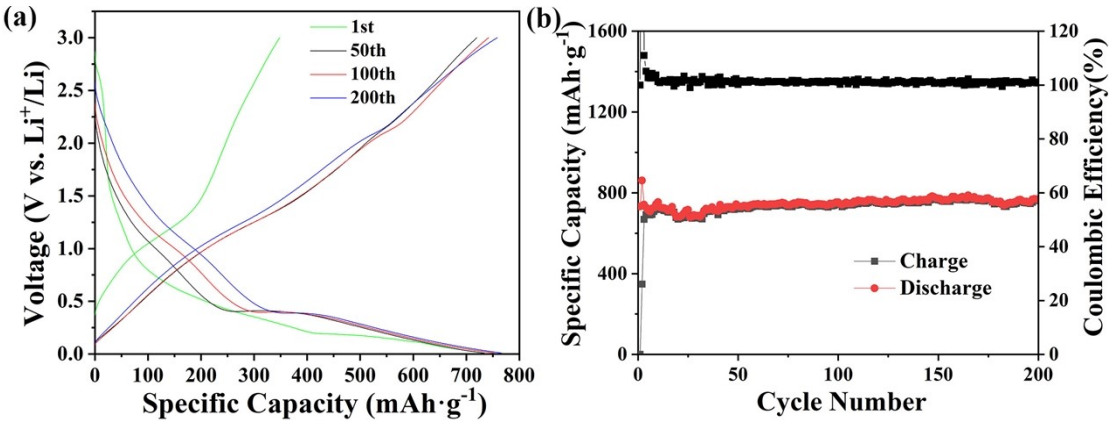

Figure S11. (a) Charge/discharge curves of the first, 50, 100, and 200 cycles of MnO@Void@NC at a current density of 0.5 A g^{-1}; (b) Cycle performance graph of MnO@Void@NC at a current density of 0.5 A g^{-1}.

Explanation: Figure S11a is the charge-discharge curve of the sample MnO@Void@NC at a current density of 0.5 A g^{-1}. In the first circle, the specific discharge capacity and the specific charge capacity in the figure are 732.76 mAh g^{-1} and 348.05 mAh g^{-1}, respectively. Its Coulomb efficiency is 47.50%. This is caused by the SEI film formed in the first circle, and the discharge capacity of the material continues to increase in the subsequent cycles. The discharge specific capacity of the 50th, 100th, and 200th laps are 733.93, 752.77, 766.38 mAh g^{-1}, and it can be seen from Figure S11b that the subsequent cycles maintain a high cycle efficiency.

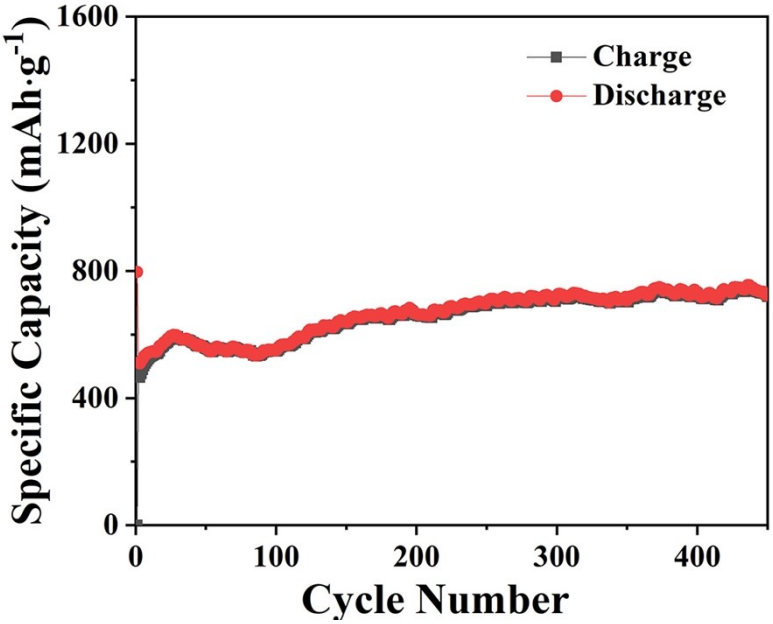

Figure S12. 450 cycling performance of MnO@Void@NC at the current density of 1 A g^{-1}.

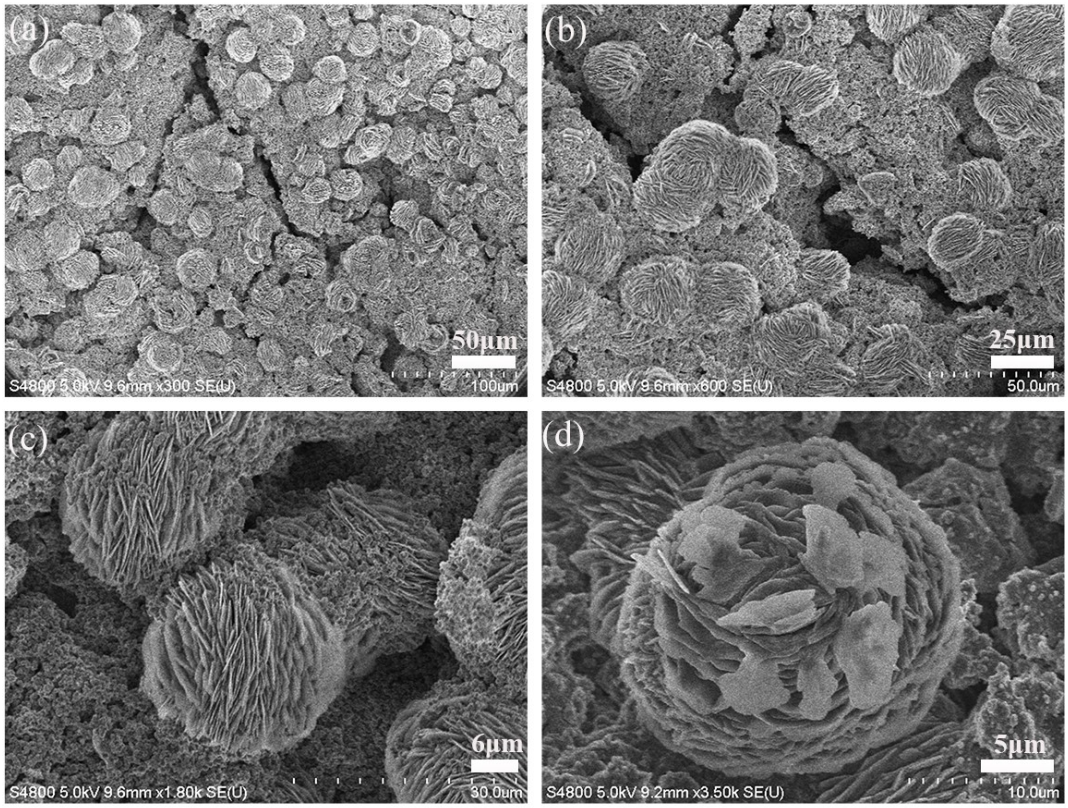

Figure S13. SEM images of the material MnO@Void@NC after 400 cycles at 0.2 A g^{-1}.

Table S1. The comparison of the specific surface area of present work with reported MnO/C composite.

Samples	Specific surface area (m^2g^{-1})	References
MnO/C nanorods	175.23	1
MnO@NC microspheres	76.0	2
Pod-like MnO@NC nanorods	61.7	3
Sandwich-like CNT@MnO@N-doped carbon hetero-nanotubes	157.6	4
Porous MnO@NC microspheres	76.54	5
RGO-MnO@NC	85.8	6
YS-MnO@NC	203	7
Cauliflower-like MnO/NC	86.9	8
MnO/NC nanospheres	24.6	9
MnO@Void@NC	194.4	This work

Table S2. The comparison of the capacity of present work with reported MnO/C composite.

Materials	Current density ($A\ g^{-1}$)	Cycle number	Capacity ($mAh\ g^{-1}$)	Ref
MnO/C hybrid	0.2	400	814	10
MnO/nanodendrites/rGO	0.2	75	1081.5	11
MnO/carbon pyrolysis	0.1	100	1066	12
MnO/C nanotubes	0.2	190	680.7	13
MnO/N-doped carbon /rGO	0.1	70	864.7	14
MnO/C aerogel	0.2	140	1177.7	15
MnO/N-C	0.5	200	890	16
MnO/Carbon fifibers	0.08	100	780	17
MnO/C nanopeapods	0.5	100	1119	18
MnO@Void@NC	0.2	200	1143.9	This work

References

1. Zhang, X. J.; Zhu, G.; Yan, D.; Lu, T.; Pan, L. K., MnO@C nanorods derived from metal-organic frameworks as anode for superiorly stable and long-life sodium-ion batteries. *J Alloy Compd* **2017,** *710*, 575-580.

2. Zhang, P. L.; Liu, J. Z.; Zhou, C. C.; Guo, S. Z.; Li, S.; Yang, Y.; Wu, J.; Yu, D.; Chen, H. F.; Zhao, M.; Chen, L. Y., Polypyrrole-derived nitrogen-doped carbon coated hierarchical MnO porous microspheres for highly reversible lithium storage. *J Electroanal Chem* **2020,** *856*, 113733.

3. Wang, Y. J.; Chen, X. C.; Liu, Z. F.; Wu, H.; Zhao, H.; Liu, H.; Zhang, Y., Cycling-induced structure refinement of MnO nanorods wrapped by N-doped carbon with internal void space for advanced lithium-ion anodes. *Appl Surf Sci* **2019,** *479*, 386-394.

4. Wang, Y. J.; Wu, H.; Liu, Z. F.; Zhao, H.; Huang, L.; Wang, Q.; Liu, H.; Zhang, Y., Tailoring sandwich-like CNT@MnO@N-doped carbon hetero-nanotubes as advanced anodes for boosting lithium storage. *Electrochim Acta* **2019,** *304*, 158-167.

5. Gou, Q. Z.; Li, C.; Zhong, W. L.; Zhang, X. Q.; Dong, Q.; Lei, C. X., Hierarchical structured porous N-doped carbon coating MnO microspheres with enhanced electrochemical performances as anode materials for lithium-ion batteries. *Electrochim Acta* **2019,** *296*, 730-737.

6. Wang, Y. J.; Wu, H.; Liu, Z. F.; Zhao, H.; Liu, H.; Zhang, Y., Bottom-Up Construction of Reduced-Graphene-Oxide-Anchored MnO with an Nitrogen-Doped Carbon Coating for Synergistically Improving Lithium-Ion Storage. *Inorg Chem* **2018,** *57* (21), 13693-13701.

7. Qin, Y. M.; Jiang, Z. Q.; Rong, H. B.; Guo, L. P.; Jiang, Z. J., High performance of yolk-shell structured MnO@nitrogen doped carbon microspheres as lithium ion battery anode materials and their in operando X-ray diffraction study. *Electrochim Acta* **2018,** *282*, 719-727.

8. Chen, T.; Wu, Z. G.; Xiang, W.; Wang, E. H.; Chen, T. R.; Guo, X. D.; Chen, Y. X.; Zhong, B. H., Cauliflower-like MnO@C/N composites with multiscale, expanded hierarchical ordered structures as electrode materials for Lithium- and Sodium-ion batteries. *Electrochim Acta* **2017,** *246*, 931-940.

9. Zhang, L. L.; Ge, D. H.; Qu, G. L.; Zheng, J. W.; Cao, X. Q.; Gu, H. W., Formation of porous nitrogen-doped carbon-coating MnO nanospheres for advanced reversible lithium storage. *Nanoscale* **2017,** *9* (17), 5451-5457.

10. Wang, S. B.; Xing, Y. L.; Liu, X.; Xu, H. Z.; Zhang, S. C., Sustainable carbon-sheets and their

MnO-C hybrid for Li-ion batteries. *RSC Adv* **2016,** *6* (82), 79066-79071.

11. Liu, B. L.; Li, D.; Liu, Z. J.; Gu, L. L.; Xie, W. H.; Li, Q.; Guo, P. Q.; Liu, D. Q.; He, D. Y., Carbon-wrapped MnO nanodendrites interspersed on reduced graphene oxide sheets as anode materials for lithium-ion batteries. *Appl Surf Sci* **2017,** *394*, 1-8.

12. Ma, J. J.; Wang, H. J.; Liu, X. R.; Lu, L. D.; Nie, L. Y.; Yang, X.; Chai, Y. Q.; Yuan, R., Synthesis of tube shape MnO/C-P composite from 3,4,9,10-perylenetetracarboxylic dianhydride for lithium ion batteries. *Chem Eng J* **2017,** *309*, 545-551.

13. Zhang, S. Z.; He, W.; Zhang, X. D.; Yang, X. N., Rational design of carbon-coated hollow MnO nanotubes for Li-ion batteries. *J Mater Sci-Mater El* **2015,** *26* (4), 2189-2197.

14. Zhang, W.; Li, J. N.; Zhang, J.; Sheng, J. Z.; He, T.; Tian, M. Y.; Zhao, Y. F.; Xie, C. J.; Mai, L. Q.; Mu, S. C., Top-Down Strategy to Synthesize Mesoporous Dual Carbon Armored MnO Nanoparticles for Lithium-Ion Battery Anodes. *ACS Appl Mater Inter* **2017,** *9* (14), 12680-12686.

15. Liu, R.; Chen, X. H.; Zhou, C. L.; Li, A.; Gong, Y.; Muhammad, N.; Song, H. H., Controlled synthesis of porous 3D interconnected MnO/C composite aerogel and their excellent lithium-storage properties. *Electrochim Acta* **2019,** *306*, 143-150.

16. Sun, Q. J.; Zhou, L.; Sun, L. S.; Wang, C. L.; Wu, Y. Q.; Wang, X. X.; Wang, L. M.; Ming, J., Bioinspired Architectures and Heteroatom Doping To Construct Metal-Oxide-Based Anode for High-Performance Lithium-Ion Batteries. *Chem-Eur J* **2018,** *24* (63), 16902-16909.

17. Zeng, S. W.; Zhao, R. R.; Li, A. J.; Xu, S. D.; Lv, D. S.; Luo, Q.; Shu, D.; Chen, H., MnO/Carbon fibers prepared by an electrospinning method and their properties used as anodes for lithium ion batteries. *Appl Surf Sci* **2019,** *463*, 211-216.

18. Jiang, H.; Hu, Y. J.; Guo, S. J.; Yan, C. Y.; Lee, P. S.; Li, C. Z., Rational Design of MnO/Carbon Nanopeapods with Internal Void Space for High-Rate and Long-Life Li-Ion Batteries. *ACS Nano* **2014,** *8* (6), 6038-6046.